Engineering Micro Oxygen Factory to Slow Tumor Progression by Hyperoxia Microenvironment

Weili Wang
Soochow University
Huizhen Zheng
Soochow University
Jun Jiang
Soochow University
Zhi Li
First Affiliated Hospital of Soochow University
Meng Gao
Soochow University
Xiaoming Cai
Soochow University
Tian Xia
University of California Los Angeles
Ruibin Li (liruibin@suda.edu.cn)
Soochow University https://orcid.org/0000-0001-6471-7658

Article

Keywords: Photosynthesis, Alginate microcapsule, Hypoxia, Tumor microenvironment, Cyanobacteria, Immunotherapy

Posted Date: May 4th, 2021

DOI: https://doi.org/10.21203/rs.3.rs-453169/v1

Version of Record: A version of this preprint was published at Nature Communications on August 2nd, 2022. See the published version at https://doi.org/10.1038/s41467-022-32066-w.

Engineering Micro Oxygen Factory to Slow Tumor Progression by Hyperoxia Microenvironment

Weili Wang [1]†, Huizhen Zheng [1]†, Jun Jiang [1], Zhi Li [2], Meng Gao [1], Xiaoming Cai [3], Tian Xia [4], Ruibin Li [1]*

[1] State Key Laboratory of Radiation Medicine and Protection, School for Radiological and Interdisciplinary Sciences (RAD-X), Collaborative Innovation Center of Radiation Medicine of Jiangsu Higher Education Institutions, Soochow University; Suzhou, Jiangsu 215123, China.

[2] Department of Interventional Radiology, the First Affiliated Hospital of Soochow University, Soochow University; Suzhou, Jiangsu 215001, China.

[3] School of Public Health, Soochow University; Suzhou, Jiangsu 215123, China.

[4] California Nanosystems Institute, University of California; Los Angeles, California 90095, United States.

†Equal contributions to this paper

*Correspondence to

Dr. Ruibin Li Email: liruibin@suda.edu.cn

Tel: +86-512-65880062

Abstract

While hypoxia promotes carcinogenesis, tumor aggressiveness, metastasis, and resistance to oncological treatments, the impacts of hyperoxia on tumors are rarely explored because *in vivo* long-lasting oxygen supply is a big challenge. Herein, we constructed a micro oxygen factory, namely photosynthesis microcapsules (PMCs) by encapsulation of acquired cyanobacteria and upconversion nanoparticles in alginate microcapsules. This system enabled long-lasting oxygen supply by converting external radiations into red emissions for photosynthesis in cyanobacteria. PMC treatment suppressed NF-kB pathway, HIF-1α production and cancer cell proliferation. Hyperoxia microenvironments created by *in vivo* PMC implants inhibited hepatocarcinoma growth and metastasis, synergized the effects of anti-PD-1 in breast cancer. The engineered oxygen factory offers potential for tumor biology study in hyperoxia microenvironments and will inspire the exploration of oncological treatments.

Key Words: Photosynthesis, Alginate microcapsule, Hypoxia, Tumor microenvironment, Cyanobacteria, Immunotherapy.

Introduction

Two hypotheses including atavism and somatic selection were raised to elucidate carcinogenesis from an evolutionary perspective[1, 2]. While the somatic selection hypothesis holds that carcinogenesis results from an accumulation of mutations by natural selections, atavism was perceived to be a revolutionary regression, by which the cancer cells act like their single-celled ancestors to shed their sophisticated characteristics, *e.g.* programmed cell deaths[3]. As low oxygen (O_2) level is a prominent characteristic in Precambrian period of single cells, the atavistic nature of cancer cells could be documented by the Warburg effect[4], namely that cancer cells prefer metabolism *via* glycolysis rather than oxidative phosphorylation pathways. Concomitantly, hypoxia microenvironment, as a hallmark of malignant tumors, has been reported to be not only the primary barrier shielding the tumor from various therapies by creating immunosuppression environment[5], activation of DNA repairment pathway[6] and autophagic flux[7], but also a promoter of carcinogenesis[8], tumor invasiveness and metastasis[9, 10]. These findings inspired the explorations of technologies to convert hypoxia into hyperoxia microenvironments for tumor biology or therapy studies.

It is a big challenge to construct a long-lasting hyperoxia microenvironment in tumors due to the lack of constant and biocompatible oxygen sources. Considering that algae microbes are the major suppliers of O_2 on earth, photosynthesis in algae chloroplasts could be potentially explored for O_2 supplements in tumors. Running of the photosynthetic machinery requires a matched light source emitting 650-700 nm photons. Since rare earth-based upconversion nanoparticles (UCNPs) have shown an extraordinary capability to convert bio-transparent near-infrared (NIR) lasers into visible lights[11], this material could be exploited to provide available photons in photosynthesis. We, therefore, hypothesized that a long-lasting hyperoxia microenvironment could be created by rational construction of algae microbes and UCNPs.

In this study, we pioneered a photosynthesis microcapsule (PMC) by encapsulating cyanobacteria and UCNPs in alginate microcapsule (MC), which could be fabricated by an electrostatic droplet technique. Four cyanobacterial strains were subjected to an evolutionary selection to acquire a suitable strain for the accommodation of physiological conditions. We comprehensively explored the impacts of NIR radiation, cell population and UCNP doses on O_2 production to designate an optimized formula of PMCs. The impacts of hyperoxia microenvironments created by PMCs were examined in nine cancer cell lines as well as two tumor models including orthotopic breast cancer in mice and transplanted hepatocarcinoma in rabbits.

Results

Bioengineering and characterization of PMCs

To demonstrate our hypothesis, we first attempted to engineer the proposed PMC system, including the selection of evolved algae microbes acclimatizing physiological conditions, synthesis of UCNPs compatible with photosynthesis, and encapsulation of algae microbes and UCNPs into MCs. Four parent algae microbes including spherical *Synechocystis sp.* 6803 (*S. sp.* 6803), *Chlorella ellipsoidea* (*C. ellipsoidea*), rod-shaped *Synechococcus elongates* 7942 (*S. elongate.* 7942), and boat-shaped *Scenedesmus obliquus* (*S. obliquus*) were subjected to a selective evolution for acclimation of physiological conditions by a stepwise alternation of growth conditions including temperature (25 to 37 ℃), and medium composition (BG11 to DMEM) (Fig. S1). The acclimatization could be assessed by detection of cell density based on the absorbance of chlorophyll-α at 650-700 nm[12]. As shown in Fig. 1A, while the proliferation of *S. obliquus* and *C. ellipsoidea* were significantly inhibited at temperature > 32 ℃, *S. sp.* 6803 and *S. elongate.* 7942 were able to acclimatize the temperature increments, evidenced by > 300% proliferation in 30 d culture. Stepwise changes of culture media from BG11 to DMEM allowed us to acquire an evolved *S. sp.* 6803 (*e-S. sp.* 6803) strain, which displayed > 90% activity at 37 ℃ after one month culture in DMEM (Fig. 1B). This strain was therefore selected for PMC construction. We then synthesized a series of UCNPs with different emissions by the

crystal growth method[11]. An Er^{3+} and Yb^{3+} doped $NaYF_4$ nanorod (15.3 × 30.2 nm) was found to emit strong fluorescence at 660 nm perfectly matching with the absorbance of chlorophyll-α (Fig. S2, Fig. S3), which is the prominent component responsible for photosynthesis. Next, we engineered the PMCs by encapsulation of algae microbes and UCNPs in the alginate-calcium microspheres under an electrostatic field *via* an electrostatic droplet generation system. As shown in Scheme 1, the whole process includes four steps: i) homogenous mixture of algae microbes with UCNPs in alginate sodium; ii) dispersion of alginate sodium solution into uniform droplets under electrostatic field; iii) encapsulation of UCNPs and microbes by cross-linked alginate-calcium in $CaCl_2$ solutions; iv) coating of alginate-calcium microsphere by poly-L-lysine (PLL), a water-soluble polycation that is resistant to enzymatic degradation and capable of preventing microbe leakage (Fig. S4). The resulting PMCs were examined by up-conversion luminescence microscopy. While empty MCs and algae-encapsulated MCs had no fluorescence signals, PMCs emitted strong red fluorescence under 980 nm excitation (Fig. 1C). These results indicated that the encapsulated UCNPs well sustained their optical properties. We comprehensively examined the impacts of microbe density and UCNP concentration on the photosynthetic activity of PMCs (Fig. 1D). An optimized formula of PMCs (3×10^3 algae cells and 0.67 μg UCNPs per MC) was acquired for efficient oxygen production (1.6 μg/min). The encapsulated algae microbes could survive in PMCs at the physiological condition for over one month (Fig. S5). These observations were further confirmed by the quantification data of dissolved oxygen in PMCs (Fig. 1E). As expected, the oxygen generation was dependent on the intensity and exposure time of NIR radiation, indicating a controllable oxygen supply. Consequently, the produced oxygen in PMCs by photosynthesis was assessed by 2',7'-dichlorodihydroflorescein (DCFH) staining after exposure to NIR radiation for different times[13]. Non-fluorescent DCFH could be oxidized into 2′,7′-dichlorofluorescein (DCF) emitting green fluorescence in hyperoxia conditions. As shown in Fig. 1F, intensive fluorescence signals were detected in fully constructed PMCs, whereas algae-free and UCNP-free PMCs showed limited signals.

Proliferation of tumor cells in hyperoxia conditions by PMCs

We then asked whether O_2 supply by PMCs may impact the proliferation of cancer cells. The effects of PMCs were assessed in nine cancer cell lines, including breast (MCF-7, 4T1), lung (A549), liver (HepG2, VX2), intestinal (HCT 116), pancreatic (PANC-1), stomach (MGC-803) and cervical (HeLa) cells across three mammalian species (human, mouse and rabbit), and three primary cells including mouse embryonic fibroblasts (MEF), heart and kidney cells. The cell metabolic activities were examined by a colorimetric substrate in MTS assay. To avoid the cytotoxic effects of heat in NIR radiation, the NIR exposure dose was set at 300 mW/cm^2 for 15 min (Fig. S6). Three intervals of NIR radiation were applied on PMCs in 24 h culture to create hyperoxia bio-context with oxygen levels at 1.8-5.3 mg/L. As shown in Fig. 2A, PMCs coupled with NIR (NIR-PMCs) had little cytotoxicity in three normal cells but inhibited the proliferation of eight cancer cells. Notably, the oxygen-sufficient media completely suppressed the duplications of HCT-116, HepG2, MCF-7 and 4T1 cells. We comprehensively examined the impacts of PMC integrates in detail, including MCs, algae and UCNPs on MCF-7 and HepG2 cells with or without NIR radiations. As a result, the suppression effect was mainly detected in cells under NIR-PMC treatment (Fig. 2B). To further demonstrate this point, we visualized the newly-born cancer cells by a Click-iT™ EdU proliferation assay kit, consisting of EdU (5-ethynyl-2′-deoxyuridine) that could incorporate into newly synthesized DNA and fluorescently labeled by a specific click reaction[14]. As shown in Fig. 2C, NIR-PMC treatment significantly suppressed the portion of daughter cells divided from breast cancer (MCF-7) and hepatocarcinoma (HepG2) cells, as evidenced by the reduction of EdU-positive cells (red). Notably, the hyperoxia media became invalidated once the dissolved oxygens were removed by N_2 purge (Fig. S7), suggesting that oxygens rather than metabolites from algae cells were responsible for the suppression effect of NIR-PMCs.

Since NIR-PMCs had limited effect on primary cells but significantly suppressed the

proliferation of cancer cells, we speculated that hyperoxia may specifically impact the signals in carcinogenesis pathways. We examined this in HepG2 and MCF-7 cells after NIR-PMC treatment. First of all, hypoxyprobe FITC-MAb1 was used to assess hypoxia status in cancer cells. As shown in Fig. 3A, plenty green dots were observed in untreated cells cultured at 2% O_2, indicating severe hypoxia, whereas NIR-PMC treatment elevated oxygen levels and antagonized the hypoxia status. Quantification analysis of hypoxia-inducible factor-1α (HIF-1α) in cell lysates by ELISA indicated that NIR-PMC treatment could dramatically reduce the levels of HIF-1α from 987 to 97 pg/mL in MCF-7 cells and 467 to 170 pg/mL in HepG2 cells (Fig. 3B). We then investigated the impacts of NIR-PMCs on the NF-κB pathway, which plays crucial role in cancer cell survival and proliferation by controlling the transcription of target genes[15]. NIR-PMC treated cells were subjected to immunoblotting of phosphorylated protein markers (IκBα) in the canonical NF-κB pathway. TNF-α was exploited as an inducer of phosphorylated IκBα (p-IκBα) and NF-κB activation, and this effect could be antagonized by BMS-345541 (BMS)[16]. Consistent with the cell duplication results, NIR-PMC treatment significantly suppressed the levels of phosphorylated p-IκBα, indicating inhibition of NF-κB pathway and blockage of cell duplications (Fig. 3C). These results suggested that the prominent features of cancer cells including abnormal proliferation, HIF-1α overexpression and NF-κB activation could be attenuated in hyperoxia conditions created by NIR-PMCs.

Effects of oxygen supply by PMC implants on hepatocarcinoma

Next, we examined the *in vivo* impacts of oxygen supplements on hepatocarcinoma by *in situ* implant of PMCs in livers of rabbits. To determine a safe and effective radiation dose *in vivo*, we examined the impacts of NIR radiation on skin pathological changes as well as oxygen generation. A NIR radiation dose at 900 mW/cm^2 for 20 min was selected for animal treatment as it was able to create a hyperoxia microenvironment (2.7-3.4 mg/L) and avoided hyperthermia-induced tissue damages (Fig. S8). As indicated in the treatment scheme (Fig. 4A), hepatocarcinoma-bearing

rabbits received an intratumor injection of PMCs (500 μL, 1.5×10^4) were exposed to 980 nm NIR radiation for 42 days. NIR-PMC treatment created a long-lasting hyperoxia tumor microenvironment, evidenced by a dramatic reduction of HIF-1α expression (Fig. S9). The tumor growths were examined by CT imaging for 42 days (Fig. 4B). While the tumor sizes in untreated rabbits rapidly increased to 4 cm^3 on the 14^{th} d and 16 cm^3 on the 28^{th} d, NIR-PMC treatment completely inhibited tumor growth in 14 d and displayed a slow increase of tumor sizes to 4 cm^3 on the 28^{th} day (Fig. 4C). Since the lung is the most common target organ for hepatocarcinoma metastasis[17], we also examined this organ by CT imaging. As shown in Fig. 4D, notable signs of metastases could be differentiated in the lungs of untreated tumor-bearing rabbits at 14 d, and a large number of tumor foci (51 ± 25 per lung) formed on the 28^{th} d. Notably, there were few detectable pulmonary metastases in NIR-PMC treatments even on the 42^{nd} day (Fig. 4E, Fig. S10). Consistently, liver sections of rabbits receiving NIR-PMC treatment displayed a dramatic reduction of tumor-metastasis biomarker, vascular cell adhesion molecule-1 (VCAM-1)[18] (Fig. S11). Kaplan-Meier plots for survival rate comparisons were generated by continued daily monitoring of the animals at the point of moribund status or spontaneous death. Log Rank testing demonstrated a statistically significant survival benefit ($p < 0.0019$) for the NIR-PMC treatment as compared to vehicle control (Fig. 4F). Notably, two out of ten rabbits lived longer than 140 days, and almost cured as there were no detectable tumor nodules in livers and lungs by CT imaging and *ex vivo* examination (Fig. S12). To our surprise, luminescent PMCs could still be observed in livers and maintained the spherical morphologies (Fig. S12). These results indicated that the hyperoxia microenvironment created by NIR-PMCs could greatly slow tumor progression, inhibit tumor metastasis and enhance the survival rates of hepatocarcinoma-bearing rabbits.

Combined treatment of breast cancer by PMC implants and immunotherapy in mice

Since oxygen species have been widely reported as prerequisites of immune

activation[19], we speculated that long-lasting oxygen supplements by NIR-PMCs may facilitate immunotherapy by activation of the adaptive immune responses in the tumor microenvironment. We verified this by examination of CD4, CD39, CD206 and CD73 expressions in an orthotopic breast tumor model by inoculating firefly luciferase-transfected 4T1 (fLuc-4T1) tumor cells into the breast pads of BALB/c mice. As shown in Fig. 5A, NIR-PMC treatment significantly enhanced CD4 expression and reduced CD39, CD206 and CD73 expressions in tumor sections, indicating the activations of T helper cells, B cells, natural killer (NK) cells and differentiation of M1 macrophages in the tumor microenvironment[20, 21]. Therefore, a synergistic therapeutic effect could be expected for a combined treatment of NIR-PMCs and checkpoint inhibitors. The tumor-bearing mice screened by bioluminescence imaging (BLI) were randomly separated into four groups: untreated animals (vehicle Ctrl), NIR-PMC treatment, anti-PD-1 treatment (200 μg per mouse twice a week) and co-treatment by NIR-PMCs and anti-PD-1. Fig. 5B displayed the scheme of combined treatment. As shown in Fig. 5C and 5D, rapid tumor growth could be detected in untreated tumor-bearing mice by the intensive luminescence of 4T1 cells as well as bright field images. The fast proliferation of breast cancer cells led to nutrient deficiency and cell necrosis, evidenced by the diminishing luminescence in tumor cores. While co-treatment by NIR-PMC and anti-PD-1 displayed a potent therapeutic effect, NIR-PMC and anti-PD-1 treatments merely suppressed tumor growth in the first two weeks but regained rapid growth later. This result was further confirmed by the tumor volume data. The tumor sizes in co-treatment were four-fold smaller than anti-PD-1 treatment (Fig. 5E, Fig. S13). The tumor metastases were also examined in animal lungs. As shown in Fig. 5F, while anti-PD-1 had a limited effect on tumor metastases, NIR-PMC treatment could significantly reduce tumor nodules in dissected lungs. Notably, there were no detectable pulmonary tumor metastases in the co-treatment group. We also compared the survival rates of animals in different treatments (Fig. 5G). All untreated tumor-bearing animals were either dead or in moribund status in 25 days, whereas NIR-PMC and anti-PD-1 treatments could significantly extend animal survival time

(+40%). Interestingly, no animal deaths were observed in co-treatment in 50 days, and 8 out of 10 mice could survive more than 60 days. Overall, these data suggested that the combination of PMC implants with immune checkpoint inhibitors showed a strong synergistic effect (CI = 0.23) in mice bearing breast cancer.

Discussions

Tumor therapeutic strategies rely on our understanding of the carcinogenesis mechanisms. While the somatic selection was often recognized as the prominent cause of carcinogenesis, substantial research enthusiasms have been aimed at the discovery of chemo- or physico-therapeutics to eliminate the mutant cells[6, 22]. Although millions of cancer patients have successfully extended their lives by tumor killing, the side effects, drug resistance[23] and tumor metastasis[24] have become formidable hindrances. This has necessitated a rethinking of cancer therapeutic strategies. Based on the atavism theory, cancer cells may deliberately create a hypoxia microenvironment to mimic the survival conditions of their single-celled ancestors in Precambrian period. In this regard, long-lasting antagonizing of hypoxia microenvironments in tumors may suppress cell duplication and slow tumor progression. Our findings in hepatocarcinoma rabbits well supported this hypothesis as no tumor-killing agents were included. Notably, in all ten tested animals, two rabbits were cancer free as they lived five-time longer (> 140 d) than untreated animals (average survival time ~27 d) and had no detectable tumor nodes. This finding may require more validations across different tumor models. Since interventional therapy is a conventional treatment in hepatocarcinoma patients, PMCs are a promising implant for clinical applications.

Besides hepatocarcinoma model, we examined the effects of PMCs in breast cancer-bearing mice. The effects of different constituent in PMCs were comprehensively examined. Consistent with the *in vitro* results (Fig. 2B), therapeutic effects were mainly observed in animals that received NIR-PMC treatment (Fig. S14, Fig. S15). While oxygens were reported to activate antitumor immune responses, such

as the differentiation of M2 tumor-associated macrophages (TAMs) to M1[25], activation of T cells[26] as well as NK cells by synthesis of superoxide radicals[27], a synergistic effect between PMC implants and immunotherapy could be expected. To test this feasibility, we treated the breast cancer-bearing mice with anti-PD-1 and PMC implants. Notably, PMCs displayed a strong synergistic effect to immune checkpoint inhibitors.

Tumor metastasis is a complex process, involving the dissemination of cancer cells, epithelial-mesenchymal transition, and invasion by collective migration, cancer cell circulation, interaction with immune cells, metastatic colonization, *etc*. A few biomolecules including FAT1[28], ribosomal protein[29], transmembrane protein CCDC25[30], Nrf2[31] and E-cadherin[32] were recently found to regulate the metastasis progression. Besides, hypoxia as a potent microenvironmental factor was reported to promote multiple steps (*e.g.,* invasion, migration, intravasation and extravasation) within the metastatic cascade[9]. Although tumor metastasis is the major cause of treatment failure in cancer patients and responsible for 90% of cancer-related mortality[33], there are few clinical interventions. The *in vivo* micro oxygen factory constructed in this study, however, could be potentially exploited in cancer treatments for suppression of tumor metastasis. PMC implants dramatically prevented tumor metastasis in orthotopic breast cancer and transplanted hepatocarcinoma models. The hyperoxia microenvironments created by NIR-PMCs may block cancer cell invasion by antagonizing metastasis signals[19, 34].

Conclusion

In summary, we successfully constructed an oxygen factory, PMCs, by encapsulating cyanobacteria and UCNPs in alginate-polylysine microcapsules. PMCs enabled photosynthesis under NIR radiation and provided long-lasting and controllable oxygenation in bio-contexts. The supplemented O_2 by PMCs inhibited HIF-1α production and NF-κB activation in cancer cells and dramatically prevented cancer cell duplications in a non-toxic fashion. *In vivo* hyperoxia microenvironments were

created by implants of PMCs in orthotopic hepatocarcinoma and breast tumors, and significantly inhibited tumor growths and metastases. A potent synergistic effect was demonstrated in breast cancer of mice receiving the co-treatment of PMC implants and a checkpoint inhibitor (anti-PD-1). Overall, our findings demonstrated the suppression effect of the hyperoxia microenvironment on tumor progression.

Acknowledgments

This work was supported by National Key R&D Program of China, Ministry of Science and Technology of China (2018YFE0120400, 2020YFA0710700), the grants from the National Natural Science Foundation of China (Number 21976126, 21806116).

Author Contributions

R.L. conceived the idea and designed the experiments. W.W. performed most experiments. H.Z. and J. J constructed the PMCs. H.Z. performed cell proliferation test. Z.L. performed rabbit tumor implantation experiments. J.J. contributed in mice tumor implantation experiments. M.G. contributed in cell viability test. T.X. contributed the idea of immunotherapy in the hyperoxia microenvironment. The writing of the manuscript was led by R.L. with participation from W.W.

Competing interests

The authors declare no competing financial interest

Data and materials availability

All data is available in the main text or the supplementary materials.

Supplementary Materials

Additional figures of the characterization and further experimental results. The Supporting Information is available free of charge on the Nature Publications website.

References

1. F. Thomas *et al.*, Cancer adaptations: atavism, de novo selection, or something in between? *Bioessays* **589**, 39, 8, 1700039 (2017).
2. K. J. Bussey *et al.*, Ancestral gene regulatory networks drive cancer. *Proc. Natl Acad. Sci. USA* **114**, 6160-6162 (2017).
3. Y. Fuchs *et al.*, Live to die another way: modes of programmed cell death and the signals emanating from dying cells. *Nat. Rev. Mol. Cell Biol.* **16**, 329-344 (2015).
4. R. J. DeBerardinis *et al.*, We need to talk about the warburg effect. *Nat. Metab.* **2**, 127-129 (2020).
5. D. Samanta *et al.,* Chemotherapy induces enrichment of CD47(+)/CD73(+)/PDL1(+) immune evasive triple-negative breast cancer cells. *Proc. Natl Acad. Sci. USA* **115**, 1239-1248 (2018).
6. N. Rohwer *et al.*, The growing complexity of HIF-1 alpha's role in tumorigenesis: DNA repair and beyond. *Oncogene* **32**, 3569-3576 (2013).
7. J. Cosin-Roger *et al.*, Hypoxia ameliorates intestinal inflammation through NLRP3/mTOR downregulation and autophagy activation. *Nat. Commun.* **8**, 98 (2017).
8. A. Rezaeian *et al.*, A hypoxia-responsive TRAF6–ATM–H2AX signalling axis promotes HIF1α activation, tumorigenesis and metastasis. *Nat. Cell Biol.* **19***,* 38–51(2017).
9. E. B. Rankin *et al.*, Hypoxic control of metastasis. *Science* **352**, 175-180 (2016).
10. B. Thienpont *et al.*, Tumour hypoxia causes DNA hypermethylation by reducing TET activity. *Nature* **537***,* 63–68(2016).
11. B. Zhou *et al.*, Controlling upconversion nanocrystals for emerging applications. *Nat. Nanotechnol.* **10**, 924-936 (2015).
12. A. Kume, Importance of the green color, absorption gradient, and spectral absorption of chloroplasts for the radiative energy balance of leaves. *J. Plant Res.* **130**, 501-514 (2017).
13. S. J. Xu *et al.*, Vacancies on 2D transition metal dichalcogenides elicit ferroptotic cell death. *Nat. Commun.* **11**, 3484 (2020).
14. A. Salic *et al.*, A chemical method for fast and sensitive detection of DNA synthesis in vivo. *Proc. Natl Acad. Sci. USA* **105**, 2415-2420 (2008).
15. M. S. Hayden *et al.*, Shared principles in NF-kappa B signaling. *Cell* **132**, 344-362 (2008).
16. Z. L. Hu *et al.*, Aqueous synthesized quantum dots interfere with the NF-kappa B pathway and confer anti-tumor, anti-viral and anti-inflammatory effects. *Biomaterials* **108**, 187-196 (2016).
17. S. Turajlic *et al.*, Metastasis as an evolutionary process. *Science* **352**, 169-175 (2016).
18. X. Lu *et al.*, VCAM-1 Promotes osteolytic expansion of indolent bone micrometastasis of breast cancer by engaging alpha 4 beta 1-positive

osteoclast progenitors. *Cancer Cell* **20**, 701-714 (2011).
19. S. M. Hatfield *et al.*, Immunological mechanisms of the antitumor effects of supplemental oxygenation. *Sci. Transl. Med.* **7**, pp.277ra30 (2015).
20. I. Perrot *et al.*, Blocking antibodies targeting the CD39/CD73 immunosuppressive pathway unleash immune responses in combination Cancer Therapies. *Cell Rep.* **27**, 2411-2425 (2019).
21. A. S. Kashyap *et al.*, Antisense oligonucleotide targeting CD39 improves anti-tumor T cell immunity. *J. Immunother. Cancer* **7**, 67-79, (2019).
22. Y. Chao *et al.*, Combined local immunostimulatory radioisotope therapy and systemic immune checkpoint blockade imparts potent antitumour responses. *Nat. Biomed. Eng.* **2**, 611-621 (2018).
23. N. Vasan *et al.*, A view on drug resistance in cancer. *Nature* **575**, 299-309 (2019).
24. K. J. Cheung *et al.*, A collective route to metastasis: Seeding by tumor cell clusters. *Science* **352**, 167-169 (2016).
25. M. Yang *et al.*, Diverse functions of macrophages in different tumor microenvironments. *Cancer Res.* **78**, 5492-5503 (2018).
26. J. Yan, Antitumor gamma delta T cells need oxygen to function. *Nat. Immunol.* **22**, 268-269 (2021).
27. A. Kotsafti *et al.*, Reactive oxygen species and antitumor immunity-from surveillance to evasion. *Cancers* **12**, 1748-1764 (2020).
28. I. Pastushenko *et al.*, Fat1 deletion promotes hybrid EMT state, tumour stemness and metastasis. *Nature* **589**, 448-455 (2021).
29. R. Y. Ebright *et al.*, Deregulation of ribosomal protein expression and translation promotes breast cancer metastasis. *Science* **367**, 1468-1473 (2020).
30. L. B. Yang *et al.*, DNA of neutrophil extracellular traps promotes cancer metastasis via CCDC25. *Nature* **583**, 133-138 (2020).
31. L. Lignitto *et al.*, Nrf2 activation promotes lung cancer metastasis by inhibiting the degradation of bach1. *Cell* **178**, 316-329 (2019).
32. V. Padmanaban *et al.*, E-cadherin is required for metastasis in multiple models of breast cancer. *Nature* **573**, 439-444 (2019).
33. M. Esposito *et al.*, Emerging strategies for treating metastasis. *Nat. Cancer* **2**, 258–270 (2021).
34. J. Yang *et al.*, Guidelines and definitions for research on epithelial-mesenchymal transition. *Nat. Rev. Mol. Cell Biol.* **21**, 341-352 (2020).

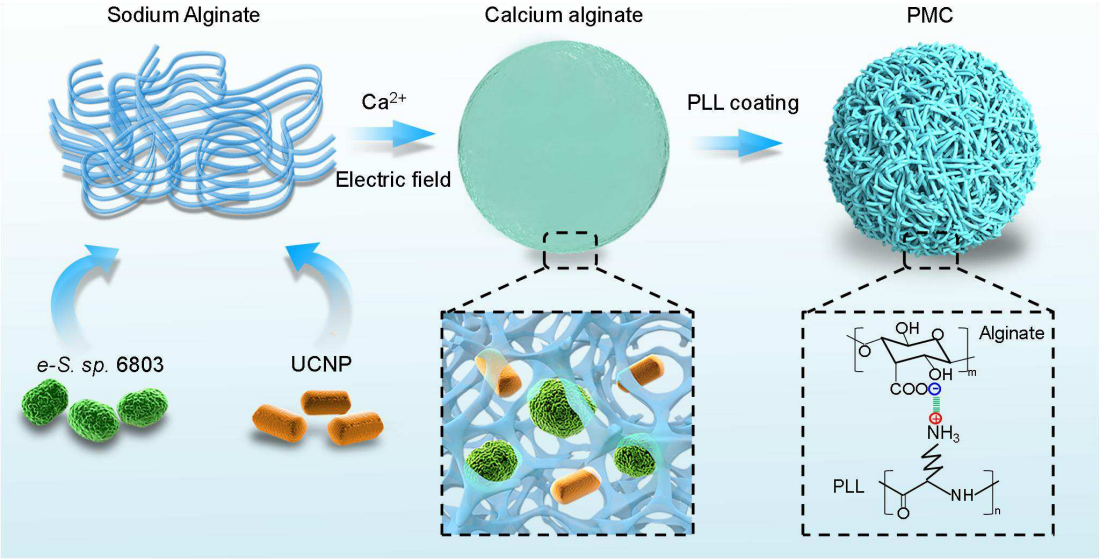

Scheme 1 Schematic image displaying the critical steps of PMC construction

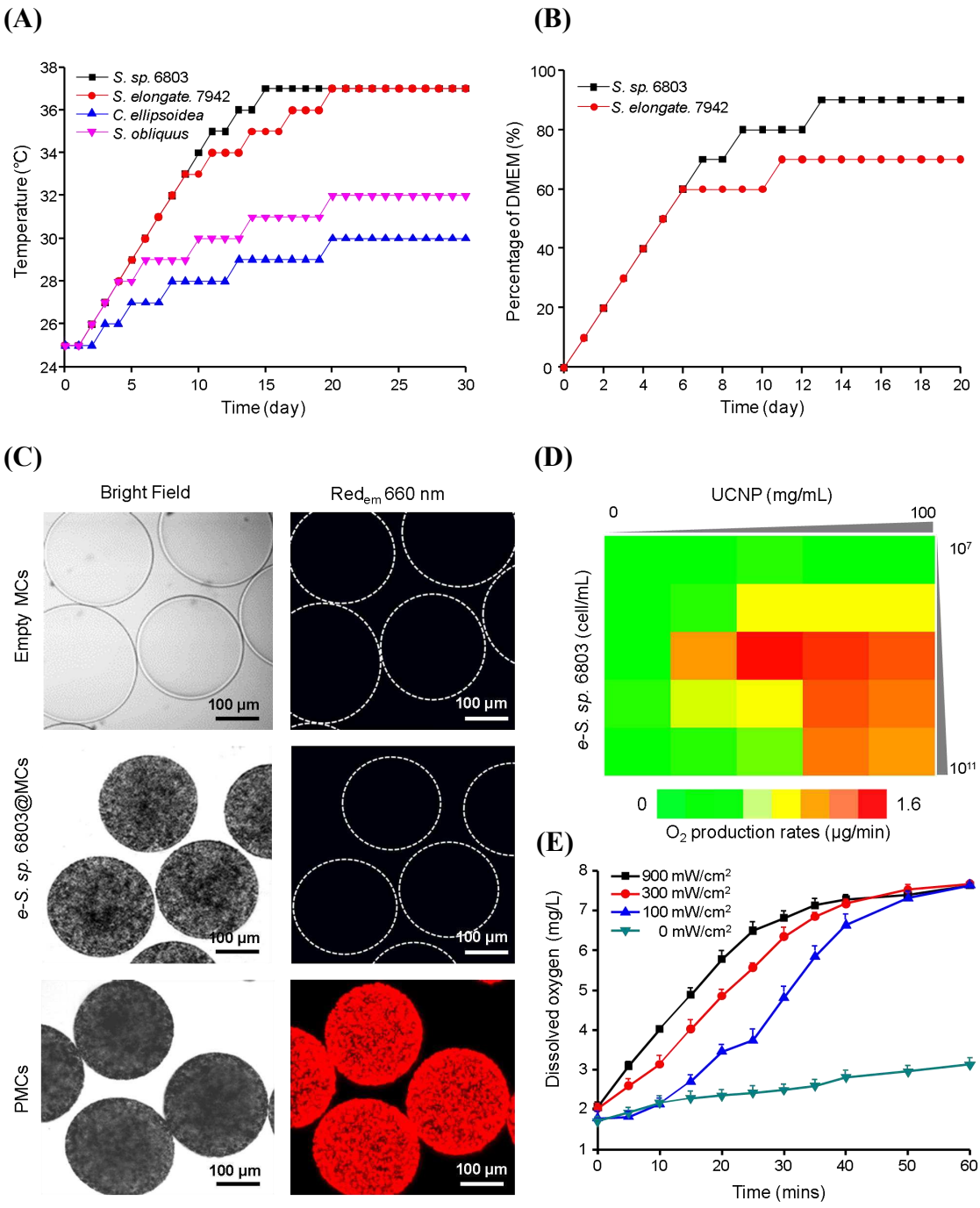
(A)
S. sp. 6803
S. elongate. 7942
C. ellipsoidea
S. obliquus
Temperature (°C)
Time (day)
(B)
S. sp. 6803
S. elongate. 7942
Percentage of DMEM (%)
Time (day)
(C)
Bright Field
Red$_{em}$ 660 nm
Empty MCs
e-S. sp. 6803@MCs
PMCs
100 μm
(D)
UCNP (mg/mL)
0
100
10^7
10^{11}
e-S. sp. 6803 (cell/mL)
0
1.6
O_2 production rates (μg/min)
(E)
900 mW/cm^2
300 mW/cm^2
100 mW/cm^2
0 mW/cm^2
Dissolved oxygen (mg/L)
Time (mins)

(F)

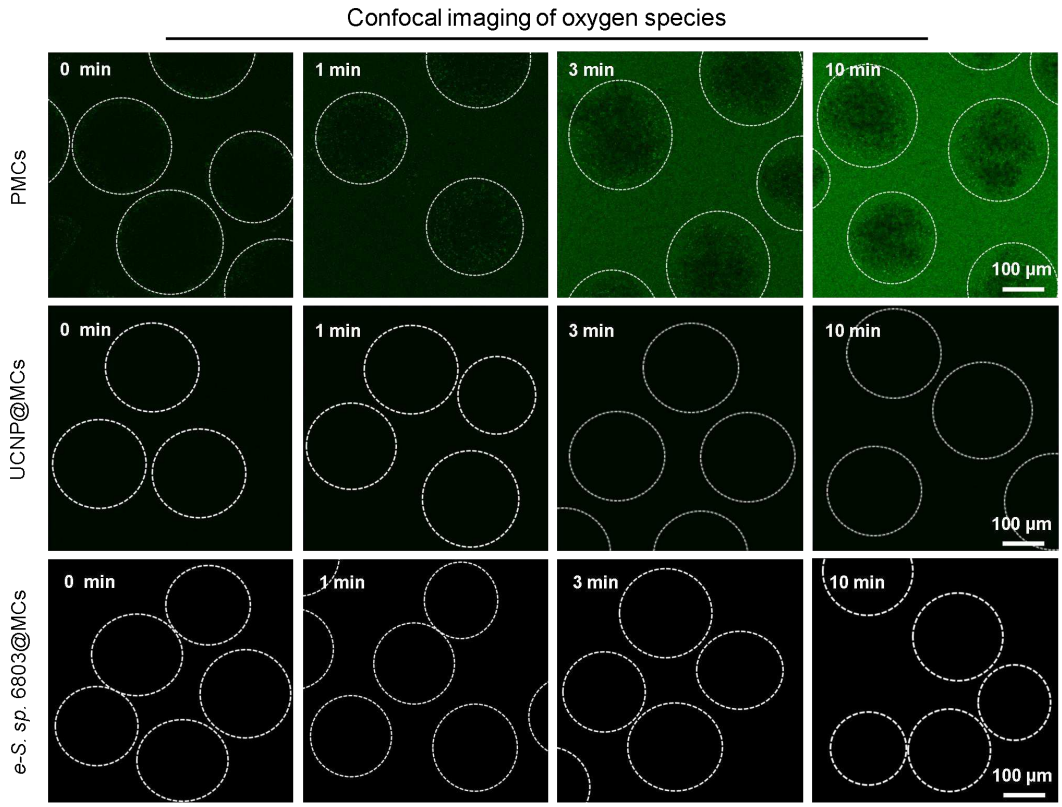

Fig. 1 Bioengineering and characterization of PMCs

Evolutional trajectory of algae strains by stepwise alternation of **(A)** temperature (25 to 37 ℃) and **(B)** medium composition from BG11 to DMEM. **(C)** Imaging of constructed PMCs. The empty MCs, MCs containing algae cells (*e-S. sp.* 6803@MCs) and fully constructed PMCs were subjected to imaging by up-conversion luminescence microscopy at 980 nm. **(D)** A heatmap presenting O_2 productions by PMCs with different formulations. Algae cells at 10^7-10^{11} cell/mL, UCNPs at 0-100 mg/mL were mixed with 1 mL alginate sodium to prepare different formulations of PMCs by an electrostatic droplet generation system. The resulting PMCs were exposed to 900 mW/cm^2 NIR radiation for 20 min to detect O_2 levels by a portable dissolved oxygen meter. **(E)** Impacts of NIR radiation on O_2 synthesis by PMCs. PMCs at 3000/mL were exposed to 100, 300 and 900 mW/cm^2 NIR radiations for O_2 detections. Data are presented as means ± SD, n = 3 independent experiments. **(F)** Visualization of synthesized O_2 in PMCs by DCFH staining. PMCs, *e-S. sp.* 6803@MCs and UCNP@MCs cultured in dark for 12 h were incubated with 10 μg/mL DCFH for 10 min and then exposed to 300 mW/cm^2 980 nm NIR radiation for 0, 1, 3 and 10 min. The treated microspheres were immediately visualized by confocal microscopy at 488 nm excitation.

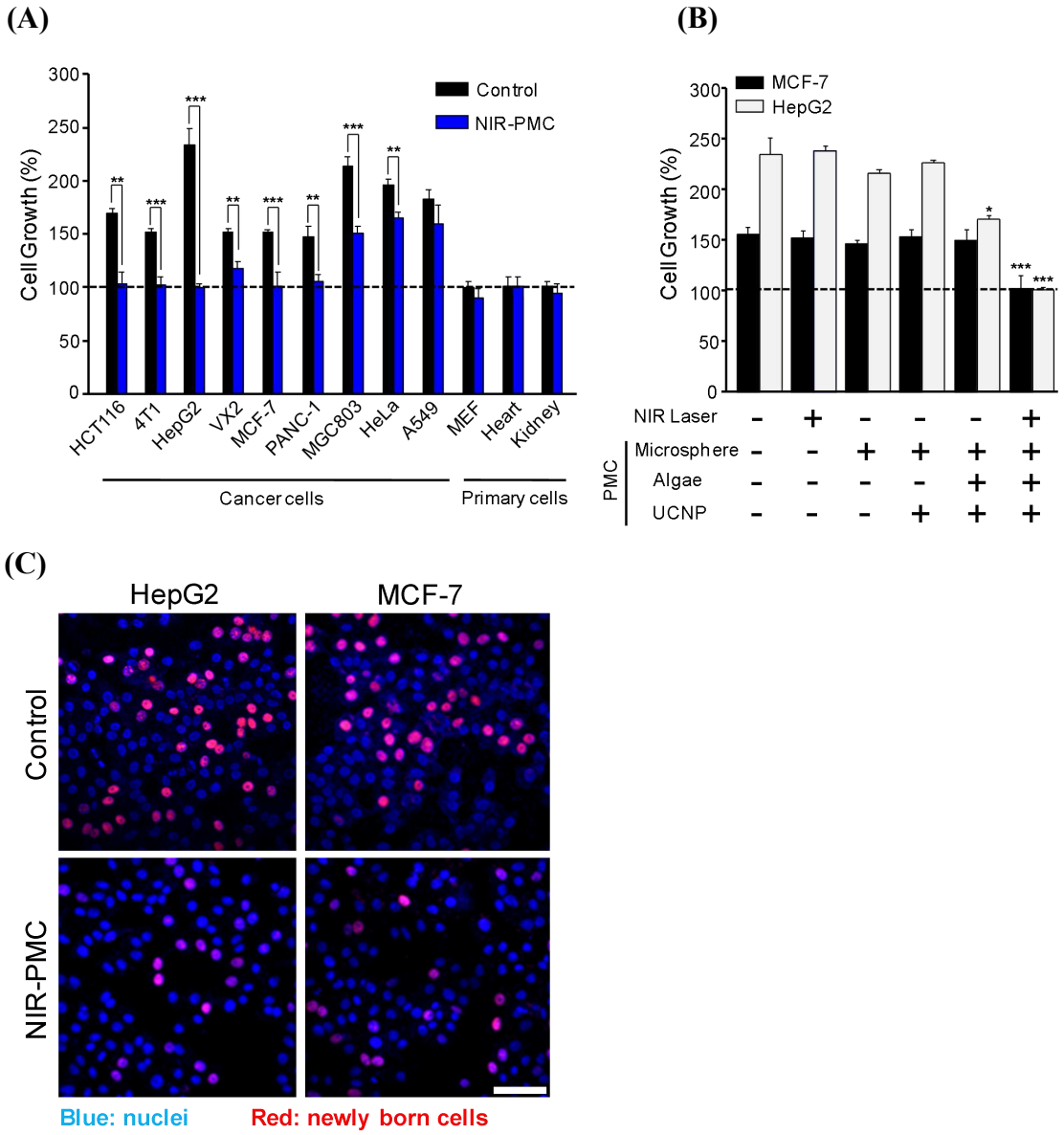

Fig. 2 Impacts of NIR-PMCs on cancer cell proliferation

(A) Cell proliferation assessment. HCT116, 4T1, HepG2, VX2, MCF-7, PANC-1, MGC-803, HeLa, A549, MEF, primary heart and kidney cells incubated with or without PMCs (500/well) were exposed to 300 mW/cm^2 NIR radiation for three intervals. After 24 h, the cell viability was examined by MTS assay (n = 6 biologically independent cell samples). Data are presented as means ± SD. ***$p < 0.001$ and **$p < 0.01$ compared to Ctrl cells by two-tailed Student t-test. **(B)** Impacts of integrates in PMCs. MCF-7 and HepG2 cells were incubated with MCs, UCNP@MCs, *e-synechocystis*@MCs and PMCs in the presence or absence of NIR radiations for cell viability assessment (n = 6 biologically independent cell samples). Data are presented as mean ± SD. ***$p < 0.001$ and *$p < 0.05$ compared to control group by two-tailed Student t-test. **(C)** Confocal visualization of newly born cells. HepG2 and MCF-7 cells after NIR-PMC treatment were stained by BeyoClick-iT® EdU-594 assay kit (scale bar: 20 μm) for confocal imaging.

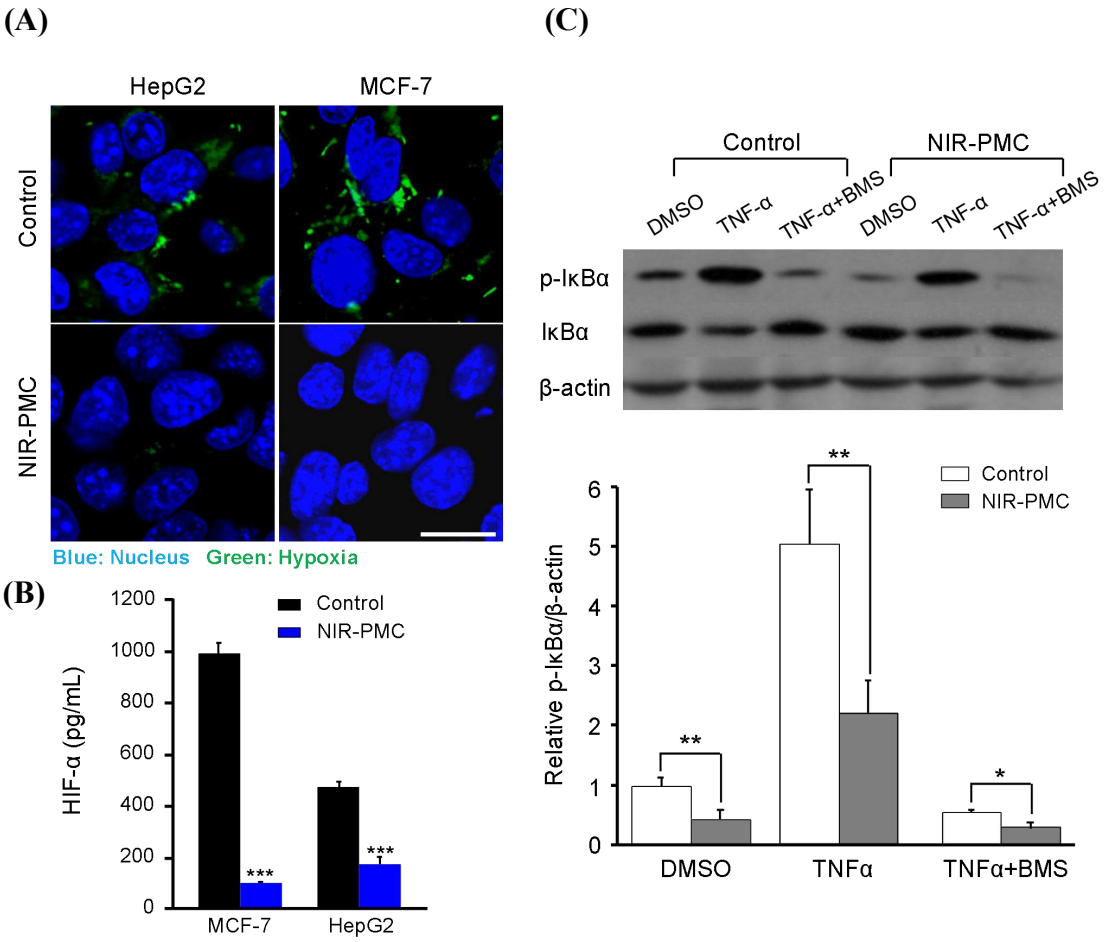

Fig. 3 Assessment of cellular HIF-1α and NF-κB in hyperoxia culture

(A) Confocal imaging of hypoxic status in cells. HepG2 and MCF-7 cells cultured in hypoxic condition were incubated with or without PMCs, followed by NIR radiation for 45 min (300 mW/cm^2). The treated cells were stained with Hypoxyprobe^{TM}-1 Plus Kit (scale bar: 10 μm) for confocal imaging. **(B)** Quantification of HIF-α in cells. HepG2 and MCF-7 cells cultured at hypoxic condition were subjected to NIR-PMC treatment for 45 min (300 mW/cm^2). The cell lysates were collected for HIF-1α quantification by ELISA (n = 3 biologically independent cell samples). Data are expressed as mean ± SD. ***$p < 0.001$ compared to Ctrl cells by two-tailed Student t-test. **(C)** Immunoblotting images of IκBα in treated cells. MCF-7 cells pretreated with BMS (20 nmol/mL), DMSO for 2 h or 200 ng/mL TNF-a for 10 min were treated by NIR-PMCs for 24 h. Cell lysates were collected and subjected to Western blotting analysis of IκBα and phosphorylated IκBα. The ratios of p-IκBα *v.s.* β-actin were determined by Image J 1.51. Data are presented as mean values ± SD. **$p < 0.01$ and *$p < 0.05$ compared to Ctrl cells by two tailed Student t-test.

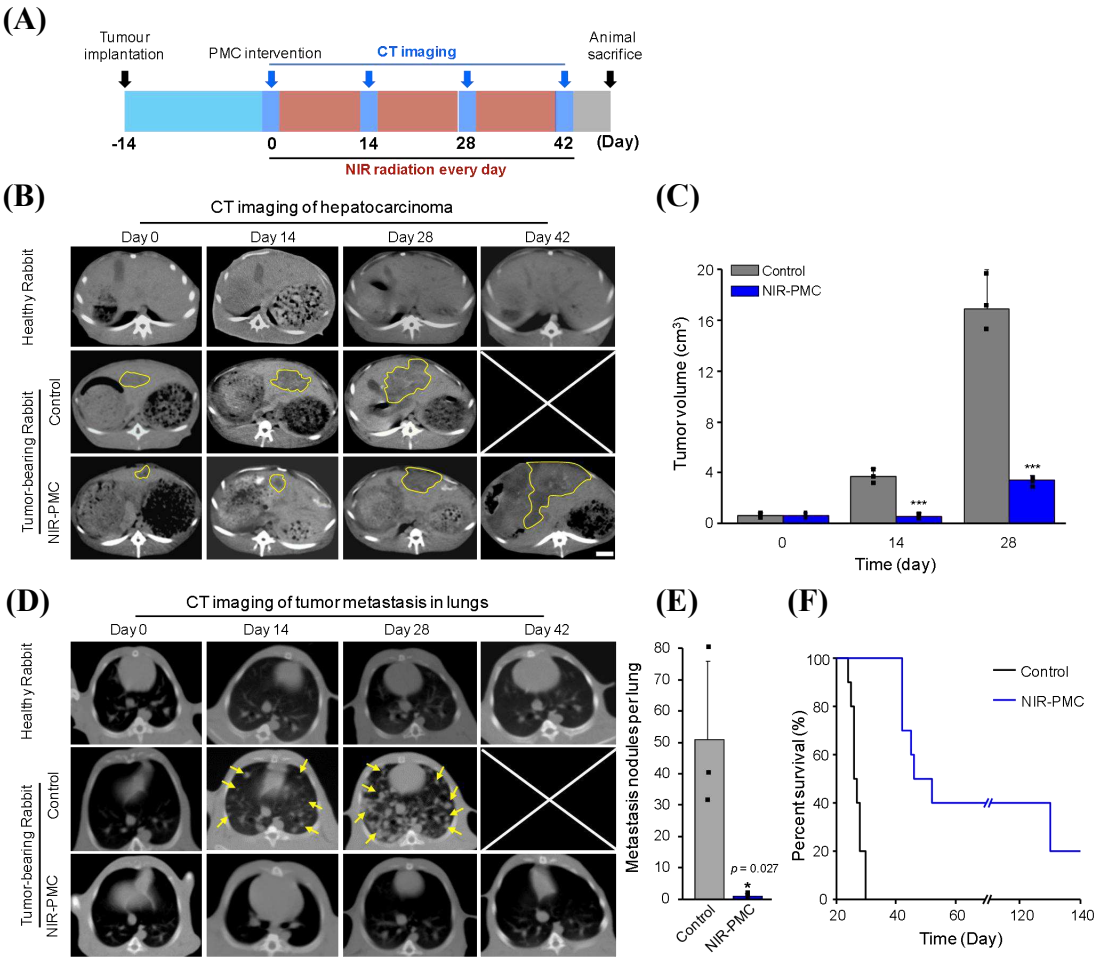

Fig. 4 Effects of hyperoxia microenvironment by PMC implants in rabbit hepatocarcinoma

(A) Schematic illustration of NIR-PMC treatment in hepatocarcinoma tumor-bearing rabbits. At 14 day post tumor implantation (tumor sizes ~ 1 cm^3), 1.5×10^4 PMCs (0.5 mL) were intratumorally injected into tumor-bearing rabbits, followed by 900 mW/cm^2 NIR radiation for 42 days. **(B)** Representative axial CT images of tumor growth. Tumor-bearing rabbits were treated with or without NIR-PMCs. The healthy, tumor-bearing and NIR-PMC treated animals were subjected to CT imaging (MHCT brilliance 16, Philips, Holland) at 0, 14, 28, 42 day. The shape/edge of hepatocarcinoma tumors are described by yellow outline (Scale bars, 1 cm). **(C)** Measurement of tumor sizes by CT images. The sizes of hepatocarcinoma tumors were measured by Neusoft PACS/Ris V5.5 at 28 d post treatment (n = 3). Data are presented as mean ± SD. ***$p < 0.001$, compared to untreated hepatocarcinoma rabbits by two tailed Student t-test. **(D)** Representative axial CT images of pulmonary tumor metastases. The animal lungs were imaged by CT at 0, 14, 28, 42 day post treatment. The nodules of pulmonary metastases are described by yellow arrow. **(E)** The numbers of pulmonary metastases nodules in rabbit lungs (n = 3). Data are presented as mean ± SD. *$p < 0.05$ compared to untreated animals by two tailed Student t-test. **(F)** Kaplan-Meier curves showing the survival rates of the indicated rabbits in 140 days (n = 10).

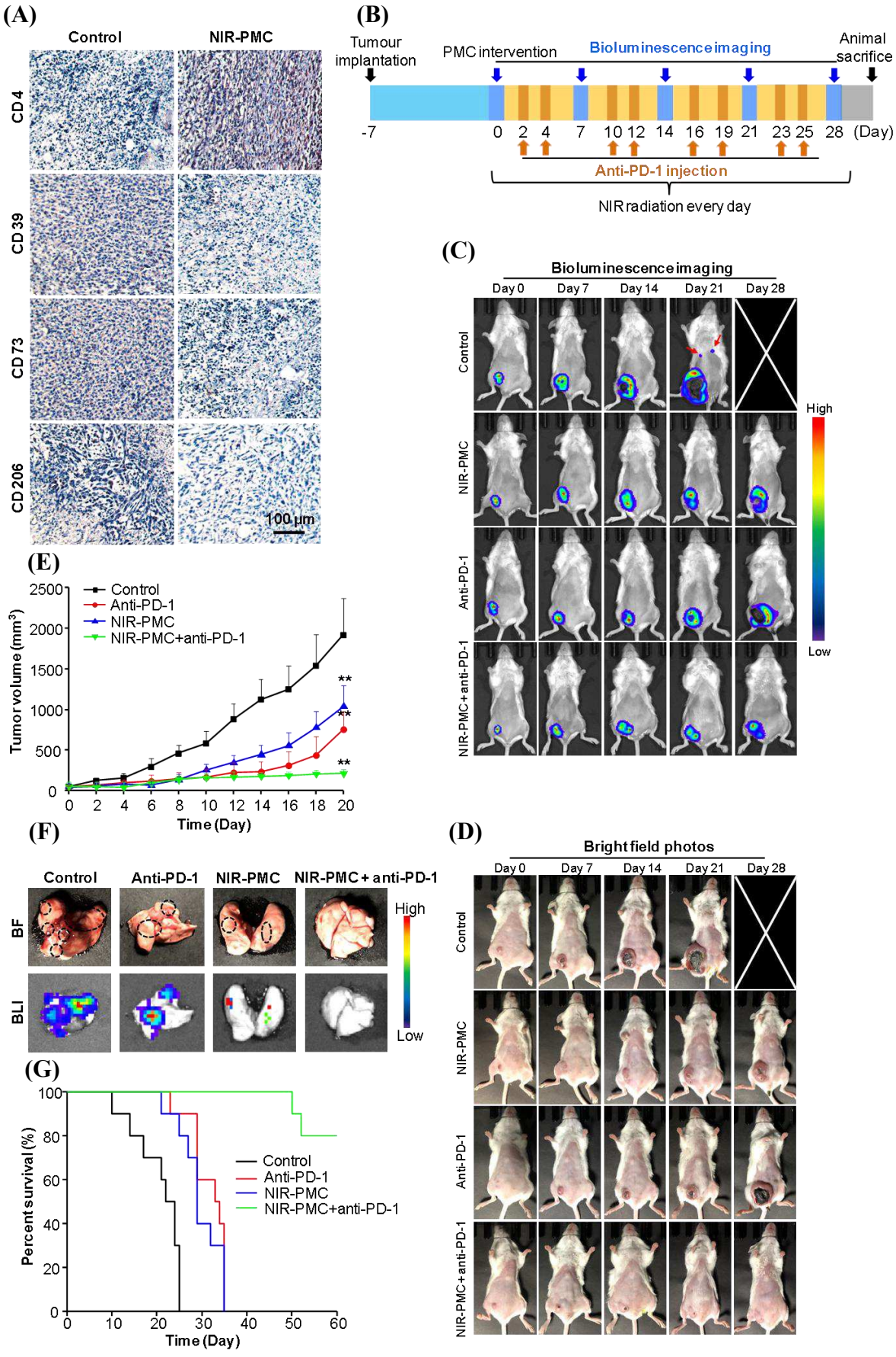
(A)
Control
NIR-PMC
CD4
CD39
CD73
CD206
100 μm
(B)
Tumour implantation
PMC intervention
Bioluminescence imaging
Animal sacrifice
-7
0 2 4 7 10 12 14 16 19 21 23 25 28 (Day)
Anti-PD-1 injection
NIR radiation every day
(C)
Bioluminescence imaging
Day 0
Day 7
Day 14
Day 21
Day 28
Control
NIR-PMC
Anti-PD-1
NIR-PMC+anti-PD-1
High
Low
(D)
Bright field photos
Day 0
Day 7
Day 14
Day 21
Day 28
Control
NIR-PMC
Anti-PD-1
NIR-PMC+anti-PD-1
(E)
Control
Anti-PD-1
NIR-PMC
NIR-PMC+anti-PD-1
Tumor volume (mm3)
Time (Day)
**
(F)
Control
Anti-PD-1
NIR-PMC
NIR-PMC + anti-PD-1
BF
BLI
High
Low
(G)
Percent survival (%)
Time (Day)
Control
Anti-PD-1
NIR-PMC
NIR-PMC+anti-PD-1

Fig. 5 Therapeutic effects of NIR-PMCs combined with anti-PD-1 in breast cancer mice

(A) Representative images of immunohistochemical staining (CD4, CD39, CD206 and CD73) of breast tumors. **(B)** Schematic illustration of combined treatment by NIR-PMCs and anti-PD-1. At 7 d post tumor implantation (tumor size ~ 100 mm^3), 750 PMCs (25 μL) were intratumorally injected in tumor-bearing mice, followed by 300 mW/cm^2 NIR radiation for 28 days. Each mouse received 10 mg/Kg anti-PD-1 twice a week. **(C)** Bioluminescence and **(D)** bright field images of breast-cancer bearing mice. Animals received different therapeutic agents were subjected to bioluminescence imaging by IVIS imaging spectrum system at 0, 7, 14, 21, 28 day. **(E)** Average tumor growth curves of mice. Tumor volume of individual mice was measured by vernier caliper every 2 days for 20 days (n = 10). Data are presented as mean ± SD. $^{**}p < 0.01$, compared to untreated breast cancer mice by two tailed Student t-test. **(F)** *Ex vivo* imaging of pulmonary metastasis. The animals received different treatments were sacrificed at 21 d for visualization of metastasis nodules in lungs. **(G)** Kaplan-Meier curves showing the survival rates of the indicated mice in 60 days (n = 10).

Figures

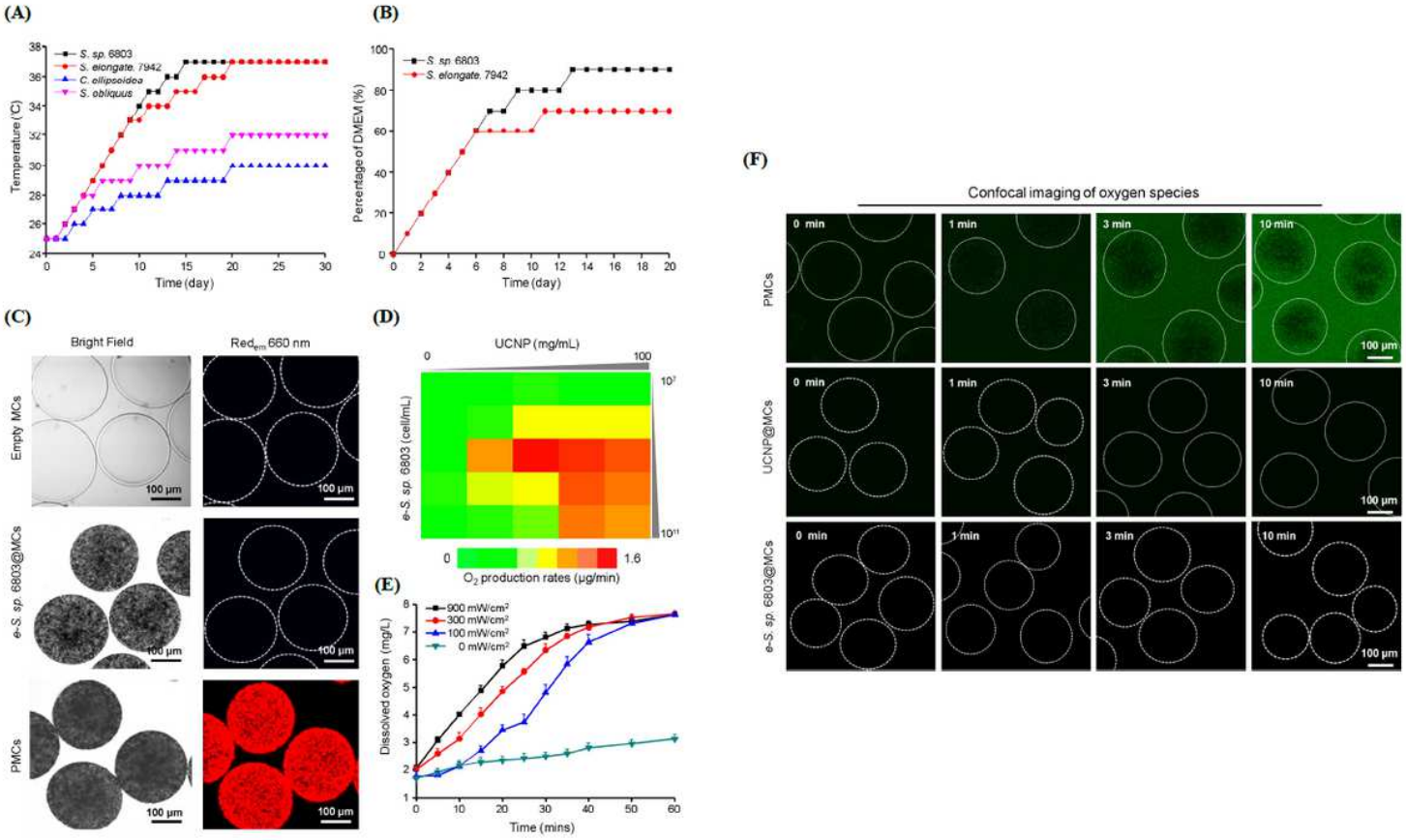

Figure 1

Bioengineering and characterization of PMCs Evolutional trajectory of algae strains by stepwise alternation of (A) temperature (25 to 37 ℃) and (B) medium composition from BG11 to DMEM. (C) Imaging of constructed PMCs. The empty MCs, MCs containing algae cells (e-S. sp. 6803@MCs) and fully constructed PMCs were subjected to imaging by up-conversion luminescence microscopy at 980 nm. (D) A heatmap presenting O2 productions by PMCs with different formulations. Algae cells at 107-1011 cell/mL, UCNPs at 0-100 mg/mL were mixed with 1 mL alginate sodium to prepare different formulations of PMCs by an electrostatic droplet generation system. The resulting PMCs were exposed to 900 mW/cm2 NIR radiation for 20 min to detect O2 levels by a portable dissolved oxygen meter. (E) Impacts of NIR radiation on O2 synthesis by PMCs. PMCs at 3000/mL were exposed to 100, 300 and 900 mW/cm2 NIR radiations for O2 detections. Data are presented as means ± SD, n = 3 independent experiments. (F) Visualization of synthesized O2 in PMCs by DCFH staining. PMCs, e-S. sp. 6803@MCs and UCNP@MCs cultured in dark for 12 h were incubated with 10 μg/mL DCFH for 10 min and then exposed to 300 mW/cm2 980 nm NIR radiation for 0, 1, 3 and 10 min. The treated microspheres were immediately visualized by confocal microscopy at 488 nm excitation.

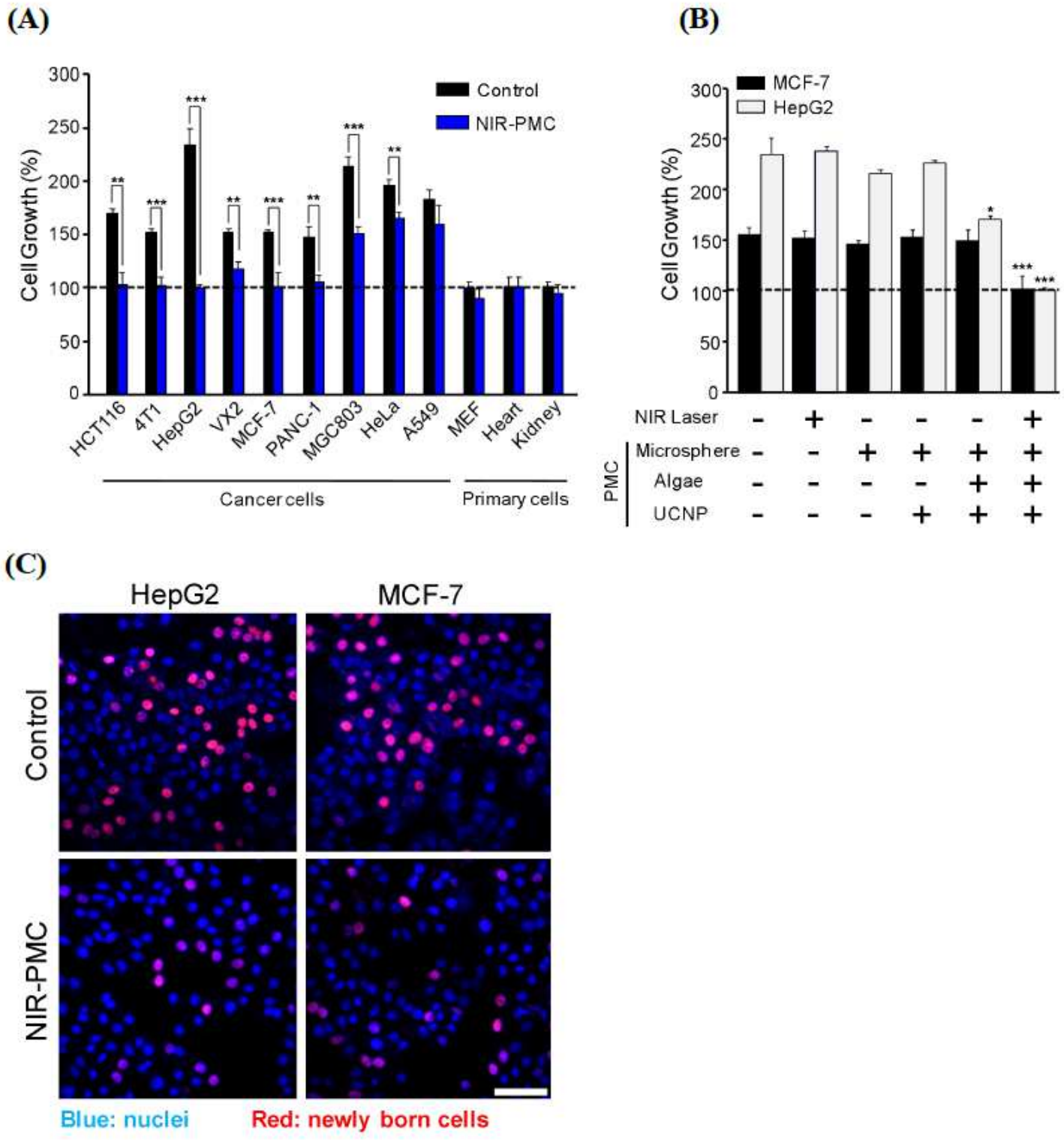

Figure 2

Impacts of NIR-PMCs on cancer cell proliferation (A) Cell proliferation assessment. HCT116, 4T1, HepG2, VX2, MCF-7, PANC-1, MGC-803, HeLa, A549, MEF, primary heart and kidney cells incubated with or without PMCs (500/well) were exposed to 300 mW/cm2 NIR radiation for three intervals. After 24 h, the cell viability was examined by MTS assay (n = 6 biologically independent cell samples). Data are presented as means ± SD. ***p < 0.001 and **p < 0.01 compared to Ctrl cells by two-tailed Student t-test. (B)

Impacts of integrates in PMCs. MCF-7 and HepG2 cells were incubated with MCs, UCNP@MCs, e-synechocystis@MCs and PMCs in the presence or absence of NIR radiations for cell viability assessment (n = 6 biologically independent cell samples). Data are presented as mean ± SD. ***p < 0.001 and *p < 0.05 compared to control group by two-tailed Student t-test. (C) Confocal visualization of newly born cells. HepG2 and MCF-7 cells after NIR-PMC treatment were stained by BeyoClick-iT® EdU-594 assay kit (scale bar: 20 μm) for confocal imaging.

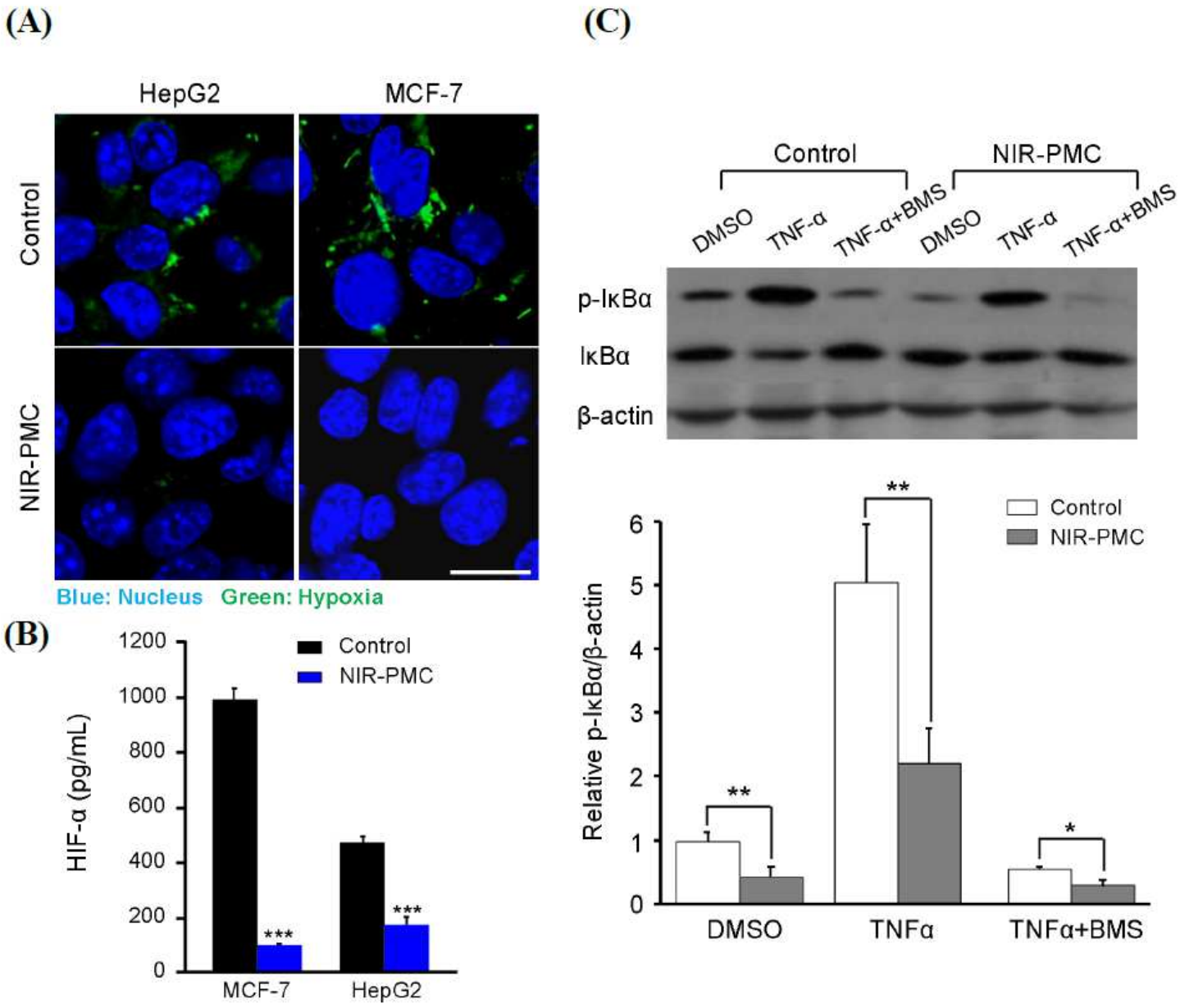

Figure 3

Assessment of cellular HIF-1α and NF-κB in hyperoxia culture (A) Confocal imaging of hypoxic status in cells. HepG2 and MCF-7 cells cultured in hypoxic condition were incubated with or without PMCs, followed by NIR radiation for 45 min (300 mW/cm2). The treated cells were stained with HypoxyprobeTM-1 Plus Kit (scale bar: 10 μm) for confocal imaging. (B) Quantification of HIF-α in cells. HepG2 and MCF-7 cells cultured at hypoxic condition were subjected to NIR-PMC treatment for 45 min

(300 mW/cm2). The cell lysates were collected for HIF-1α quantification by ELISA (n = 3 biologically independent cell samples). Data are expressed as mean ± SD. ***p < 0.001 compared to Ctrl cells by two-tailed Student t-test. (C) Immunoblotting images of IκBα in treated cells. MCF-7 cells pretreated with BMS (20 nmol/mL), DMSO for 2 h or 200 ng/mL TNF-a for 10 min were treated by NIR-PMCs for 24 h. Cell lysates were collected and subjected to Western blotting analysis of IκBα and phosphorylated IκBα. The ratios of p-IκBα v.s. β-actin were determined by Image J 1.51. Data are presented as mean values ± SD. **p < 0.01 and *p < 0.05 compared to Ctrl cells by two tailed Student t-test.

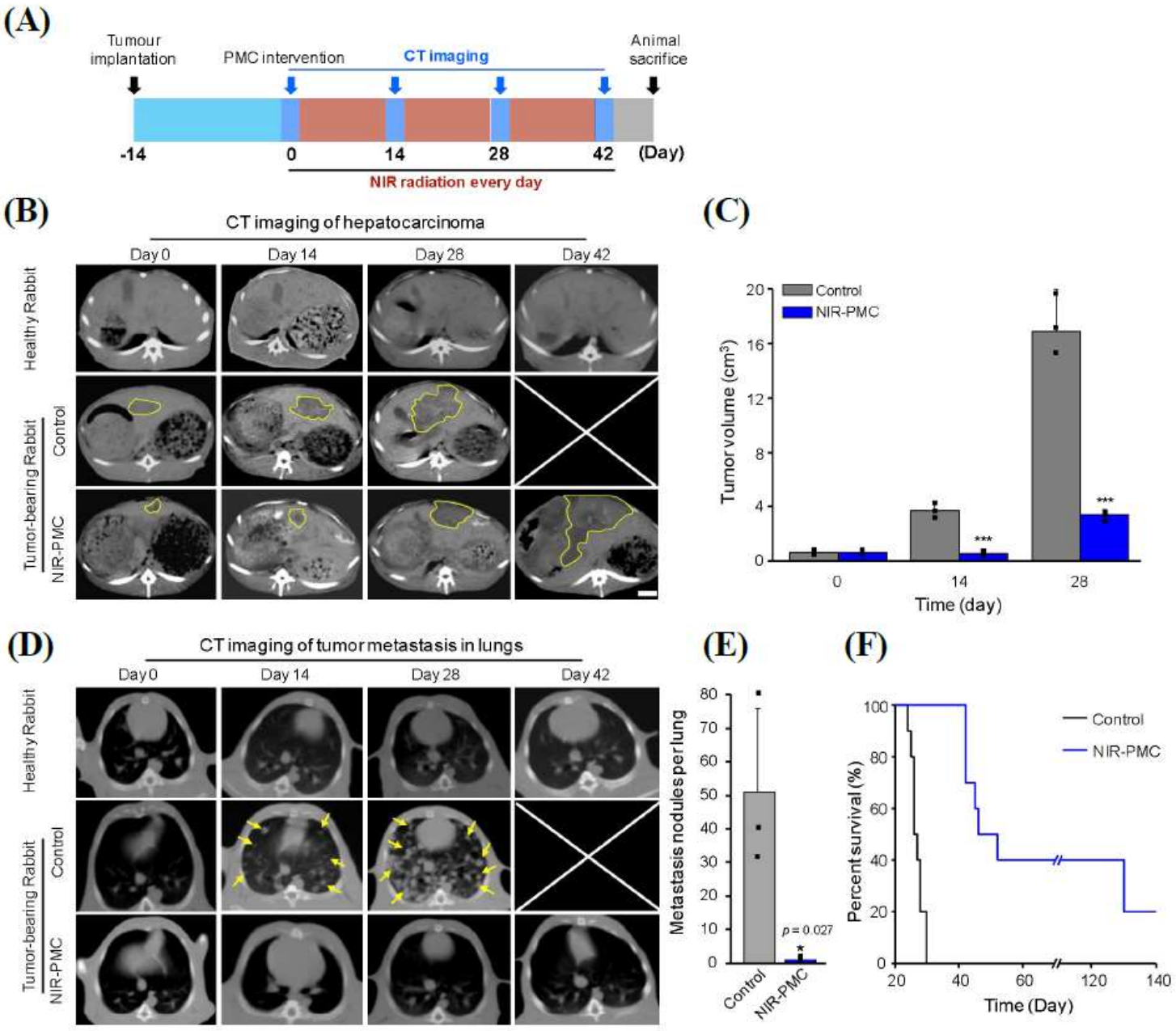

Figure 4

Effects of hyperoxia microenvironment by PMC implants in rabbit hepatocarcinoma (A) Schematic illustration of NIR-PMC treatment in hepatocarcinoma tumor-bearing rabbits. At 14 day post tumor implantation (tumor sizes ~ 1 cm3), 1.5×104 PMCs (0.5 mL) were intratumorally injected into tumor-

bearing rabbits, followed by 900 mW/cm2 NIR radiation for 42 days. (B) Representative axial CT images of tumor growth. Tumor-bearing rabbits were treated with or without NIR-PMCs. The healthy, tumor-bearing and NIR-PMC treated animals were subjected to CT imaging (MHCT brilliance 16, Philips, Holland) at 0, 14, 28, 42 day. The shape/edge of hepatocarcinoma tumors are described by yellow outline (Scale bars, 1 cm). (C) Measurement of tumor sizes by CT images. The sizes of hepatocarcinoma tumors were measured by Neusoft PACS/Ris V5.5 at 28 d post treatment (n = 3). Data are presented as mean ± SD. ***p < 0.001, compared to untreated hepatocarcinoma rabbits by two tailed Student t-test. (D) Representative axial CT images of pulmonary tumor metastases. The animal lungs were imaged by CT at 0, 14, 28, 42 day post treatment. The nodules of pulmonary metastases are described by yellow arrow. (E) The numbers of pulmonary metastases nodules in rabbit lungs (n = 3). Data are presented as mean ± SD. *p < 0.05 compared to untreated animals by two tailed Student t-test. (F) Kaplan-Meier curves showing the survival rates of the indicated rabbits in 140 days (n = 10).

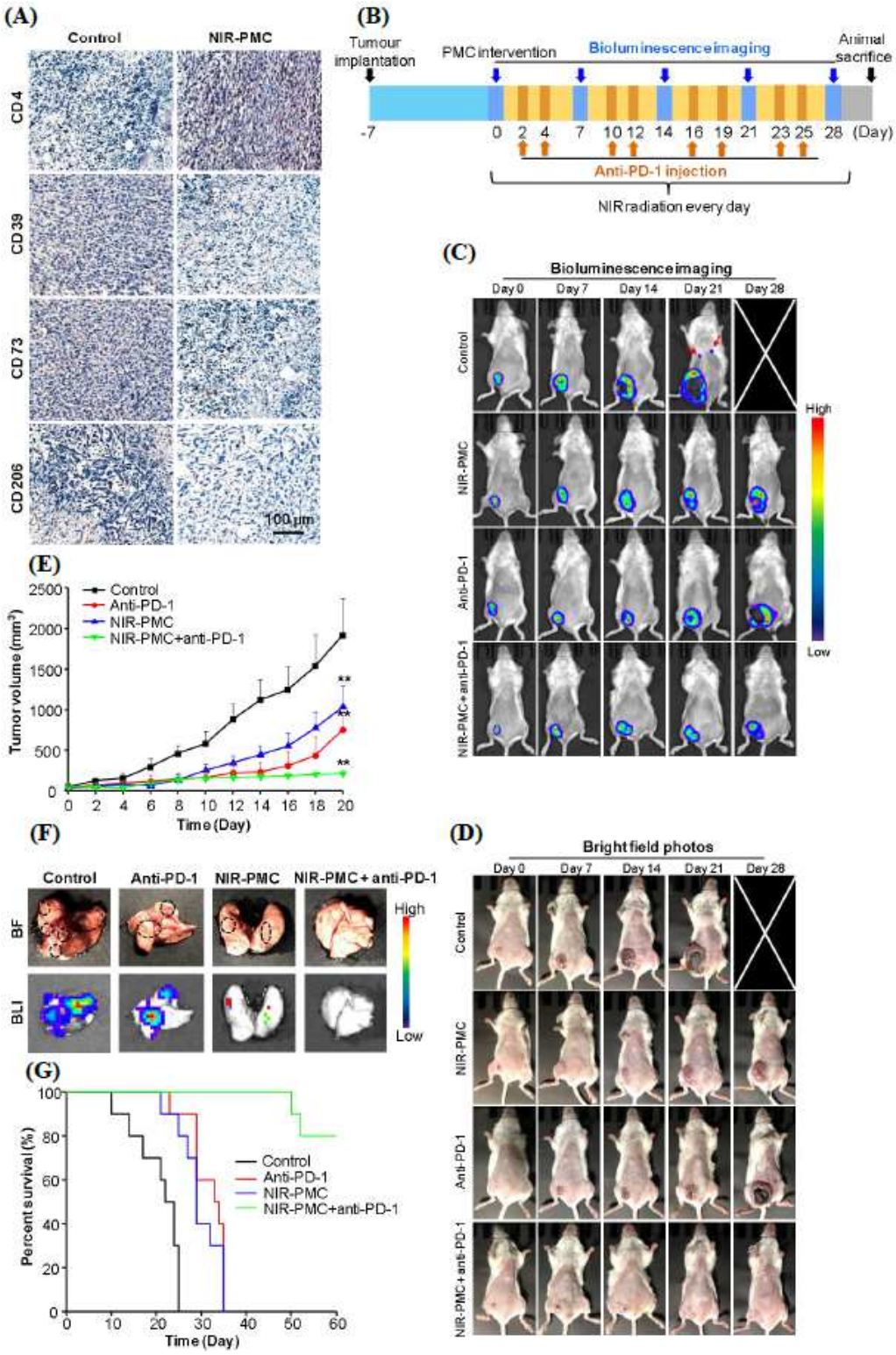

Figure 5

Therapeutic effects of NIR-PMCs combined with anti-PD-1 in breast cancer mice (A) Representative images of immunohistochemical staining (CD4, CD39, CD206 and CD73) of breast tumors. (B) Schematic illustration of combined treatment by NIR-PMCs and anti-PD-1. At 7 d post tumor implantation (tumor size ~ 100 mm3), 750 PMCs (25 μL) were intratumorally injected in tumor-bearing mice, followed by 300 mW/cm2 NIR radiation for 28 days. Each mouse received 10 mg/Kg anti-PD-1 twice a week. (C)

Bioluminescence and (D) bright field images of breast-cancer bearing mice. Animals received different therapeutic agents were subjected to bioluminescence imaging by IVIS imaging spectrum system at 0, 7, 14, 21, 28 day. (E) Average tumor growth curves of mice. Tumor volume of individual mice was measured by vernier caliper every 2 days for 20 days (n = 10). Data are presented as mean ± SD. **p < 0.01, compared to untreated breast cancer mice by two tailed Student t-test. (F) Ex vivo imaging of pulmonary metastasis. The animals received different treatments were sacrificed at 21 d for visualization of metastasis nodules in lungs. (G) Kaplan-Meier curves showing the survival rates of the indicated mice in 60 days (n = 10).

Supplementary Files

This is a list of supplementary files associated with this preprint. Click to download.

- SupportinginformationNatureBiotech.pdf